Neutron resonance spectroscopy on ^{113}Cd to E_n=15 keV

C.M. Frankle
Los Alamos National Laboratory, Los Alamos, New Mexico 87545

E.I. Sharapov and Yu.P. Popov
Joint Institute for Nuclear Research, Dubna, Russia 141980

J.A. Harvey, N.W. Hill, and L.W. Weston
Oak Ridge National Laboratory, Oak Ridge, Tennessee 37831
(Received 20 June 1994)

The results of a study of the compound nucleus ^{114}Cd by neutron time-of-flight spectroscopy methods are presented. Targets of both natural cadmium and cadmium enriched in the 113 isotope were used. The neutron total capture and neutron transmission were both measured. A total of 275 new resonances were located. In addition, 102 other resonances which were previously known but not assigned to a particular cadmium isotope were definitively assigned to ^{113}Cd. Resonance parameters E_0 and $g\Gamma_n$ were obtained for both newly identified and previously known resonances. Of the 437 resonances now known in ^{113}Cd, we identify 104 of them as $\ell = 1$ based on their small widths. Strength functions and level spacings are obtained for both $\ell = 0$ and $\ell = 1$ resonances. Comparisons of the data with Porter-Thomas reduced width distributions, Wigner nearest neighbor spacing distributions, and the Dyson-Metha Δ_3 statistic are given. The linear correlation coefficient between adjacent spacings is also discussed. The spectroscopic information obtained is of importance for planning and interpretation of parity violation measurements on the p-wave resonances of ^{113}Cd.

PACS number(s): 25.40.Ny, 27.60.+j

I. INTRODUCTION

Cadmium has been of greater than normal interest in nuclear physics practically since the discovery of the neutron in the 1930's. This was primarily due to the presence of a very strong, near thermal ($E_n = 0.178$ eV) resonance in ^{113}Cd. It was in ^{113}Cd that parity violation in highly excited nuclear states was discovered by Abov *et al.* [1] in an experiment with thermal neutrons. Cadmium also has many reasonably abundant stable isotopes. This makes it almost ideal for studies of p-wave resonances near the $3p$ maximum in the p-wave strength function.

Nonetheless, cadmium as a nucleus has not been often studied deep into the resonance region. The last major study of cadmium was of the 110, 111, 112, 113, 114, and 116 isotopes by Liou *et al.* [2] using the Nevis synchrocyclotron at Columbia University. That measurement was somewhat limited in that enriched samples were only available for the even A isotopes. As a consequence only 37 resonances were located in ^{113}Cd up to $E_n \approx 2.3$ keV. A p-wave resonance in ^{113}Cd ($E_0 = 7.0$ eV) was discovered by Alfimenkov *et al.* [3] in 1987 using the IBR-30 pulsed reactor at the Joint Institute for Nuclear Research. This resonance is responsible for Abov's parity violation effect. More recent work by Frankle *et al.* [4] located and characterized 22 additional p-wave resonances up to $E_n \approx 500$ eV using the Los Alamos Neutron Scattering Center (LANSCE) neutron spallation source. Consequently, parity violation measurements for many p-wave resonances in ^{113}Cd were initiated by the TRIPLE Collaboration as reported by Seestrom *et al.* [5]. However, the extraction of the weak matrix elements from such measurements is impossible without the knowledge of neutron resonance parameters over a broad neutron energy range.

In this paper we present the results of a study aimed at obtaining the detailed spectroscopic information on neutron resonances in ^{113}Cd. We have performed both neutron transmission and neutron total capture measurements with natural cadmium samples and with samples enriched to 94.6% in the 113 isotope. This work was performed at the Oak Ridge Electron Linear Accelerator (ORELA). (See, for example, Dabbs [6] for a description of the facility.) For practical purposes, the energy range studied was 10 eV to 3 keV in the capture reaction and 10 eV to 15 keV in transmission. Within the neutron energy region 10 eV to 15 keV we have located 275 resonances, which had not been previously identified [4,7]. In addition, we were able to assign 102 resonances, which had been listed by Mughabghab *et al.* [7] as "unassigned" to ^{113}Cd.

All 437 resonances were analyzed and their parameters (E_0 and $g\Gamma_n$) obtained by fitting with the neutron resonance analysis code SAMMY [8]. Of the total set of resonances we assign 104 of them to be $\ell = 1$ based on their small widths. A Bayes' theorem analysis [9] indicates reasonable agreement with our proposed angular momentum assignments. Strength functions and level spacings were computed for both s-wave and p-wave resonances. Additional statistical tests showed the generally high quality of the data set at lower energies. Above several keV an increasing fraction of the levels were missed and, probably, misassigned.

TABLE I. Time-of-flight (TOF) channel widths for transmission data.

Number of channels	Channel width (ns)	TOF (μs)	Energy range (eV)
16384	5	0 → 81.9	4988 →
8192	10	81.9 → 163.8	1241 → 4988
8192	20	163.8 → 327.6	310 → 1241
4096	80	327.6 → 655.3	77.3 → 310
2048	160	655.3 → 983.0	34.3 → 77.3
1024	640	983.0 → 1638	12.3 → 34.3
1024	1280	1638 → 2949	3.8 → 12.3

II. EXPERIMENTAL APPARATUS AND CONDITIONS

The Oak Ridge Electron Linear Accelerator (ORELA) [6] was used to produce a pulsed source of neutrons. Electrons of energy approximately 150 MeV strike a water cooled tantalum target producing intense bremsstrahlung γ rays. Such γ rays then generate neutrons by (γ,n) reactions. The neutrons are moderated in the water surrounding the tantalum. A detailed description of the target-moderator assembly is given by Macklin [10]. The accelerator was operated at 400 Hz during the experiment.

The transmission data were taken on ORELA flight path 1. The neutron detector was located 79.710 m from the neutron production target. Neutrons were detected with a 1 cm thick, 12.7 cm diam NE912 ^{6}Li loaded glass scintillator. The scintillator was viewed edge on by a pair of 12.7 cm photomultiplier tubes operating in coincidence. The beam intensity was monitored by a ^{235}U fission chamber located in the neutron production target room. The time-of-flight data were acquired in 40 960 channels. The breakdown of time-of-flight channel widths is shown in Table I.

Transmission data were taken in three sets, the ^{113}Cd target, the natural Cd target, and no target. Data were taken in each of these modes for about 15 min before the sample changer was moved to a different position. A ^{10}B filter was always present in the beam to remove overlap neutrons from the preceding beam bursts. In addition, data were taken with polyethylene and bismuth absorbers in order to establish the backgrounds, which were then subtracted. The final data set represents about 3 days of running time for each target. More details of standard transmission measurements can be found in the publications of the ORELA group, e.g., [11] and references therein.

The capture data were taken on ORELA flight path 7. The capture sample was located 40.110 m from the neutron production target. γ rays were detected by a pair of 1ℓ C_6D_6 detectors positioned on either side of the sample at 90° to the beam. This liquid scintillator is even less sensitive to the scattered neutrons than the nonhydrogenous scintillators used at ORELA earlier, see, e.g., [12]. The sample dimensions were 2.42 cm by 4.97 cm by 0.091 cm thick. The beam tube in the vicinity of the detectors was constructed of graphite in order to minimize the number of γ rays produced by neutrons scattered from the sample. A 1 mm thick ^{6}Li glass detector was mounted approximately 1 m upstream from the sample to monitor the beam intensity and to measure the energy dependence of the neutron flux as described earlier [13]. The time-of-flight data were acquired in 13 551 channels. The breakdown of time-of-flight channel widths is shown in Table II. These spectra were taken with an integral discriminator threshold of 150 keV. The multiparameter pulse height vs time-of-flight spectra were measured simultaneously for applying off-line pulse height weighting of capture events. The pulse height weighting procedure is often used to make the detector efficiency independent of the details of the γ-ray cascades [10]. The neutron background in our capture experiment was not studied in detail because the experiment was devised to obtain the resonance parameters for which the total count rate (the background and the nonresonance capture) between resonances must be taken as "background." We would like to remark, however, that the true background was not readily apparent in the raw data but after the weighting technique was applied it became obvious that the background in the low energy region was severe. This is because the weighting procedure gives more weight to single γ pulses corresponding to higher energies and therefore restores the bias in efficiency for registration of low multiplicity cascades typical of capture in Al, C, and Be, which

TABLE II. Time-of-flight (TOF) channel widths for capture data.

Number of channels	Channel width (ns)	TOF (μs)	Energy range (eV)
7719	16	0 → 123.5	554 →
1720	32	123.5 → 178.5	263 → 554
1173	64	178.5 → 253.6	130 → 263
860	128	253.6 → 363.7	64.0 → 130
665	256	363.7 → 533.9	29.6 → 64.0
411	512	533.9 → 744.3	15.2 → 29.6
294	1024	744.3 → 1045	7.7 → 15.2
709	4096	1045 → 3949	0.5 → 7.7

are common construction materials in standard capture measurements.

The enriched ^{113}Cd was obtained in the form of solid metal from the Russian State Pool of Stable Isotopes. An isotopic and chemical assay was provided for the ^{113}Cd samples. The enriched samples contained <0.01% ^{106}Cd, <0.01% ^{108}Cd, 0.12% ^{110}Cd, 0.16% ^{111}Cd, 1.92% ^{112}Cd, 94.60% ^{113}Cd, 2.98% ^{114}Cd, and 0.22% ^{116}Cd. Natural cadmium consists of 1.25% ^{106}Cd, 0.89% ^{108}Cd, 12.51% ^{110}Cd, 12.81% ^{111}Cd, 24.13% ^{112}Cd, 12.22% ^{113}Cd, 28.72% ^{114}Cd, and 7.47% ^{116}Cd. In the enriched samples the largest chemical contaminant was lead at 0.004%. The enriched transmission sample had a thickness of 0.0784 at/b as compared to 0.0886 at/b for the natural cadmium transmission sample. The enriched capture sample had a thickness of 0.0042 at/b as compared to 0.0037 at/b for the natural cadmium capture sample. The mass of the enriched transmission sample was 30.044 g, and the mass of the enriched capture sample was 9.452 g.

III. ANALYSIS OF THE DATA

After subtraction of the background and correction for dead time losses, the transmission was calculated for both the enriched and natural cadmium data. The data were then analyzed using the neutron resonance analysis code SAMMY [8]. The code SAMMY uses the Reich-Moore approximation [14] in the application of the R-matrix formalism. An implementation of Bayes' theorem is used to fit the requested resonance parameters to the data.

The transmission data were fit in the interval 6.3 eV to 15 keV. All other known cadmium resonances were included in the resonance analysis, a total of about 1000 resonances. Isotopic abundances were included based on the results of the aforementioned assay and were not varied. The option in the SAMMY code for the ORELA "realistic resolution function" was utilized, and the standard parameters were not varied. The Doppler width of a resonance was calculated using a free gas model with the value $T_{\rm eff}$ = 306 K for the effective temperature of the sample. The data for the ^{113}Cd target and the accompanying fit are displayed in Figs. 1 (0–5 keV) and 2 (5–15 keV). The resonance parameters extracted from the transmission data assume the values of $\Gamma_{\gamma s}$ = 100 meV and $\Gamma_{\gamma p}$ = 160 meV for the total radiative widths of the s-wave and p-wave resonances, respectively, and are listed in Table III. Note that the published table contains resonance parameters only up to 1 keV. The remainder of the table may be found in the Physics Auxiliary Publication Service (PAPS) edition of Physical Review C [15].

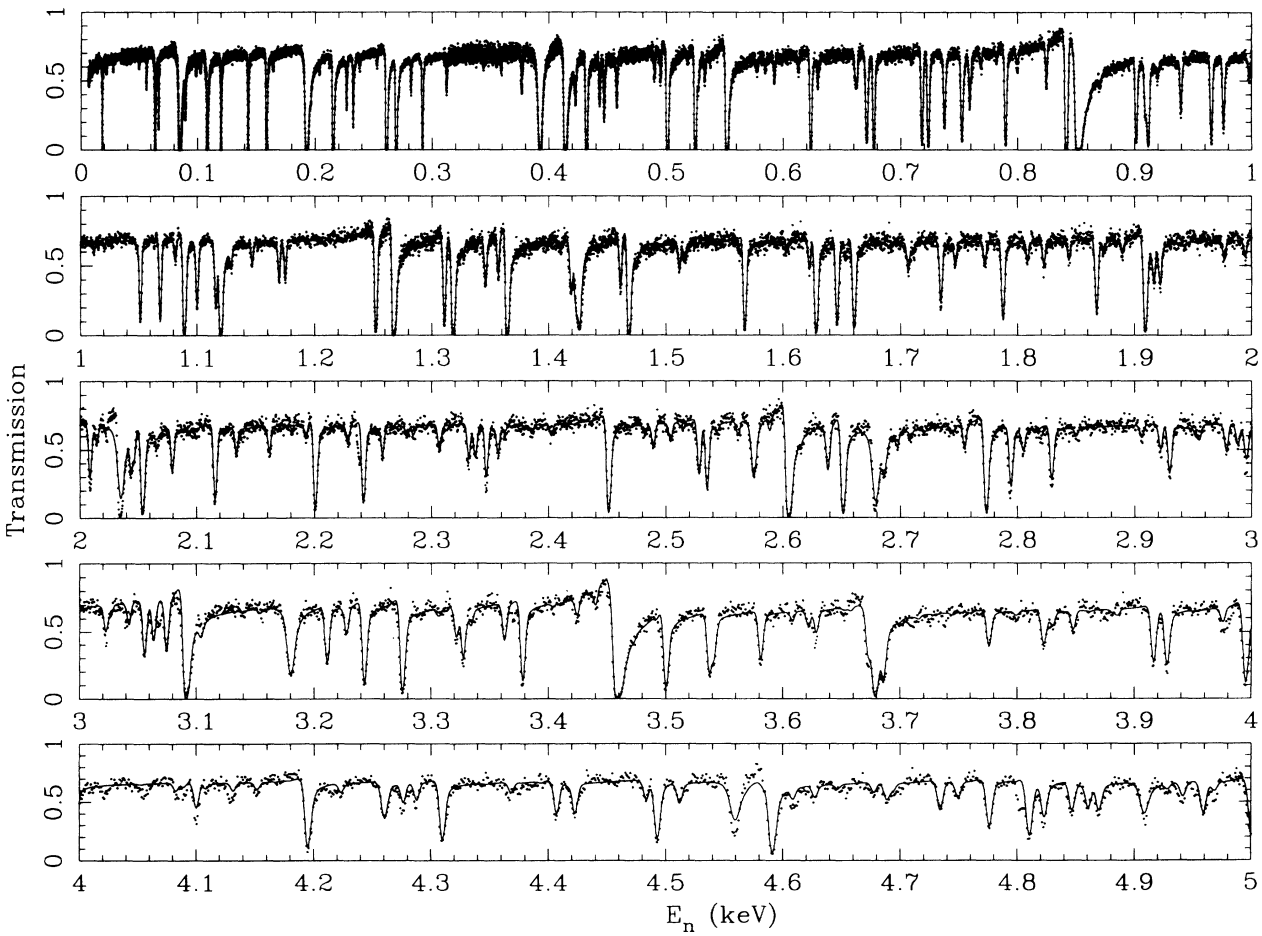

FIG. 1. ^{113}Cd transmission data and fit from 0 to 5 keV.

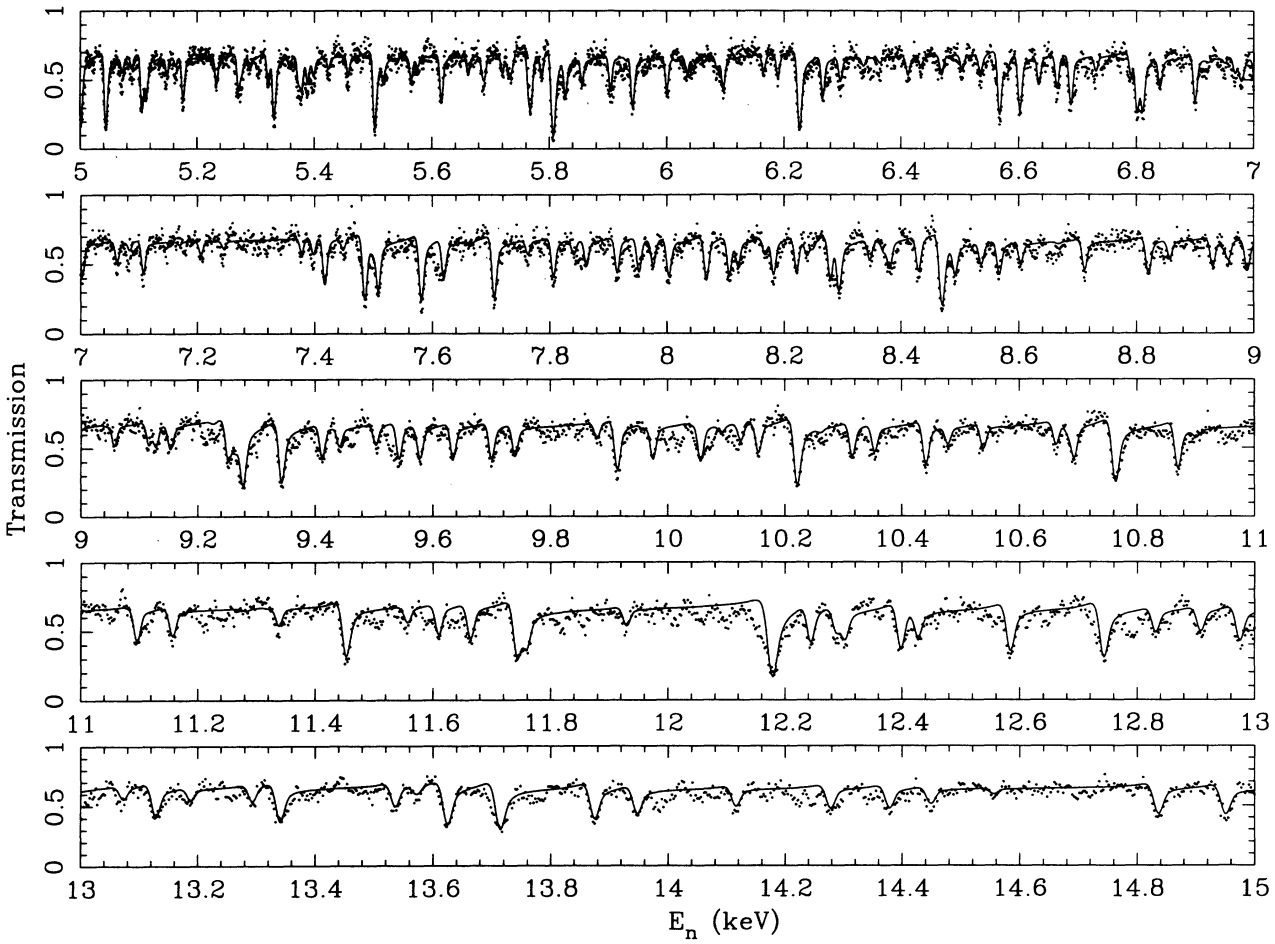

FIG. 2. ^{113}Cd transmission data and fit from 5 to 15 keV.

TABLE III. Neutron resonance parameters of ^{113}Cd from transmission and capture up to 1 keV.

E_n (eV)	$g\Gamma_n$ (meV) (transmission)	$g\Gamma_n$ (meV) (capture)
18.365±0.004	0.141 ±0.001	0.140 ±0.004
21.831±0.007	0.0071±0.0002	a
43.38 ±0.03	0.0047±0.0004	a
49.77 ±0.01	0.0154±0.0006	0.014 ±0.001
56.23 ±0.01	0.0404±0.0006	0.039 ±0.003
63.70 ±0.01	2.60 ±0.03	b
81.52 ±0.03	0.0056±0.0009	0.0053±0.0005
84.91 ±0.02	22.4 ±0.1	b
98.52 ±0.02	0.042 ±0.001	0.040 ±0.003
102.30 ±0.02	0.038 ±0.001	0.034 ±0.002
106.56 ±0.02	0.032 ±0.002	0.026 ±0.003
108.33 ±0.02	8.52 ±0.06	b
143.07 ±0.03	2.34 ±0.03	b
158.76 ±0.03	6.47 ±0.06	b
166.60 ±0.13	0.021 ±0.003	0.019 ±0.002
192.85 ±0.04	45.8 ±0.1	b
196.15 ±0.04	0.100 ±0.005	0.091 ±0.005
203.51 ±0.04	0.065 ±0.004	0.068 ±0.004
211.88 ±0.05	0.081 ±0.004	0.074 ±0.005
215.23 ±0.05	20.2 ±0.1	b
232.41 ±0.05	1.04 ±0.01	1.07 ±0.01
237.87 ±0.05	0.122 ±0.006	0.128 ±0.006

TABLE III. *(Continued).*

E_n (eV)	$g\Gamma_n$ (meV) (transmission)	$g\Gamma_n$ (meV) (capture)
252.68 ±0.05	0.133 ±0.006	0.146 ±0.006
261.07 ±0.06	26.3 ±0.2	b
269.35 ±0.06	17.5 ±0.1	b
271.50 ±0.06	0.26 ±0.01	0.26 ±0.01
281.83 ±0.06	0.477 ±0.008	0.49 ±0.01
289.64 ±0.09	0.060 ±0.008	0.06 ±0.01
291.61 ±0.06	4.40 ±0.07	b
312.30 ±0.07	0.492 ±0.009	0.49 ±0.01
343.79 ±0.07	0.16 ±0.01	0.17 ±0.01
351.61 ±0.19	0.028 ±0.008	0.037 ±0.003
359.32 ±0.08	0.26 ±0.02	0.28 ±0.01
376.82 ±0.08	0.82 ±0.01	0.86 ±0.02
385.01 ±0.12	0.08 ±0.01	0.093 ±0.007
414.05 ±0.09	94.5 ±0.4	b
422.73 ±0.09	0.99 ±0.02	1.00 ±0.02
432.01 ±0.09	18.3 ±0.2	b
447.11 ±0.09	2.10 ±0.02	2.11 ±0.03
457.75 ±0.10	1.61 ±0.02	1.64 ±0.03
489.89 ±0.10	0.70 ±0.02	0.75 ±0.03
495.08 ±0.10	0.90 ±0.02	0.92 ±0.02
501.0 ±0.1	36.9 ±0.3	b
518.3 ±0.1	0.17 ±0.03	0.21 ±0.01
524.8 ±0.1	26.1 ±0.3	b
527.4 ±0.1	0.72 ±0.02	0.71 ±0.02
533.0 ±0.1	0.77 ±0.02	0.73 ±0.03
537.5 ±0.2	0.19 ±0.03	0.18 ±0.01
543.3 ±0.3	0.15 ±0.03	0.18 ±0.01
551.9 ±0.1	79.3 ±0.5	b
577.6 ±0.1	0.35 ±0.04	0.37 ±0.02
584.7 ±0.1	0.41 ±0.04	0.48 ±0.02
592.5 ±0.1	0.84 ±0.03	0.86 ±0.03
613.0 ±0.1	0.59 ±0.03	0.58 ±0.02
623.7 ±0.1	15.4 ±0.2	b
629.9 ±0.1	1.18 ±0.03	1.21 ±0.03
661.3 ±0.1	1.01 ±0.03	1.07 ±0.03
662.9 ±0.1	1.50 ±0.04	1.42 ±0.04
677.1 ±0.3	14.9 ±0.2	b
687.6 ±0.2	0.05 ±0.03	0.06 ±0.01
709.3 ±0.2	0.32 ±0.04	0.34 ±0.02
718.2 ±0.2	11.6 ±0.2	b
723.6 ±0.2	14.7 ±0.2	b
754.0 ±0.2	0.31 ±0.03	0.37 ±0.03
759.3 ±0.2	3.60 ±0.05	3.62 ±0.05
768.9 ±0.2	0.75 ±0.05	0.78 ±0.02
782.2 ±0.2	0.34 ±0.05	0.39 ±0.02
789.8 ±0.2	14.4 ±0.3	b
824.6 ±0.2	2.65 ±0.07	2.68 ±0.06
829.4 ±0.5	0.15 ±0.04	0.12 ±0.01
841.7 ±0.2	57.5 ±0.6	b
851.7 ±0.2	401 ±1	b
870.6 ±0.2	0.85 ±0.08	0.87 ±0.03
901.4 ±0.2	14.6 ±0.2	b
911.7 ±0.2	20.0 ±0.3	b
919.7 ±0.2	0.90 ±0.08	1.03 ±0.03
939.7 ±0.2	5.1 ±0.3	b
965.5 ±0.2	13.4 ±0.2	b
976.0 ±0.2	9.1 ±0.4	b
998.0 ±0.2	1.7 ±0.1	1.56 ±0.05

[a]Not observed.

[b]$g\Gamma_n^0 > 0.15$ meV.

The new parameters should be considered a revision of the previously published ones [4], for resonances where old and new values do not agree.

The capture data were fit in the interval 6 eV to 3 keV. The broadening and resolution parameters for the fit were the same as those used for the transmission data, allowing for the difference in flight path and different detectors. The energy scale is adopted from the 80 m transmission data. The single scattering and finite size correction features of SAMMY were utilized. As was expected, the capture data are more sensitive to weak resonances than the transmission data, at least until the poorer resolution of the capture data removed the advantage. Data and fit for the capture reaction are shown in Fig. 3. The resonance parameters from the capture data are also listed in Table III. The background obscured some of the weak resonances below 100 eV. Parameters for those resonances are only from the transmission data. Though the data in between resonances in Fig. 3 were partially corrected by applying a background model to the fit within the SAMMY code, nevertheless these data do not correctly represent the off-resonance capture cross section, especially in the neutron energy region up to 300 eV, where the background is severe. In neither the transmission nor the capture data was the 7 eV resonance observed due to the use of a boron filter in the beam. Additionally, due to the difficulties in properly accounting for γ-detector saturation effects in the large resonances, widths were not extracted from the capture data for resonances with $g\Gamma_n^0 > 0.15$ meV. While this is a somewhat arbitrary cutoff, all resonances with smaller widths are properly fit. As a practical matter these are essentially the s-wave resonances. The weighted average neutron widths from both measurements and the reduced widths are given in Table IV. Note that the published table contains resonance parameters only up to 1 keV. The remainder of the table may be found in the Physics Auxiliary Publication Service (PAPS) edition of Physical Review C [15]. Note

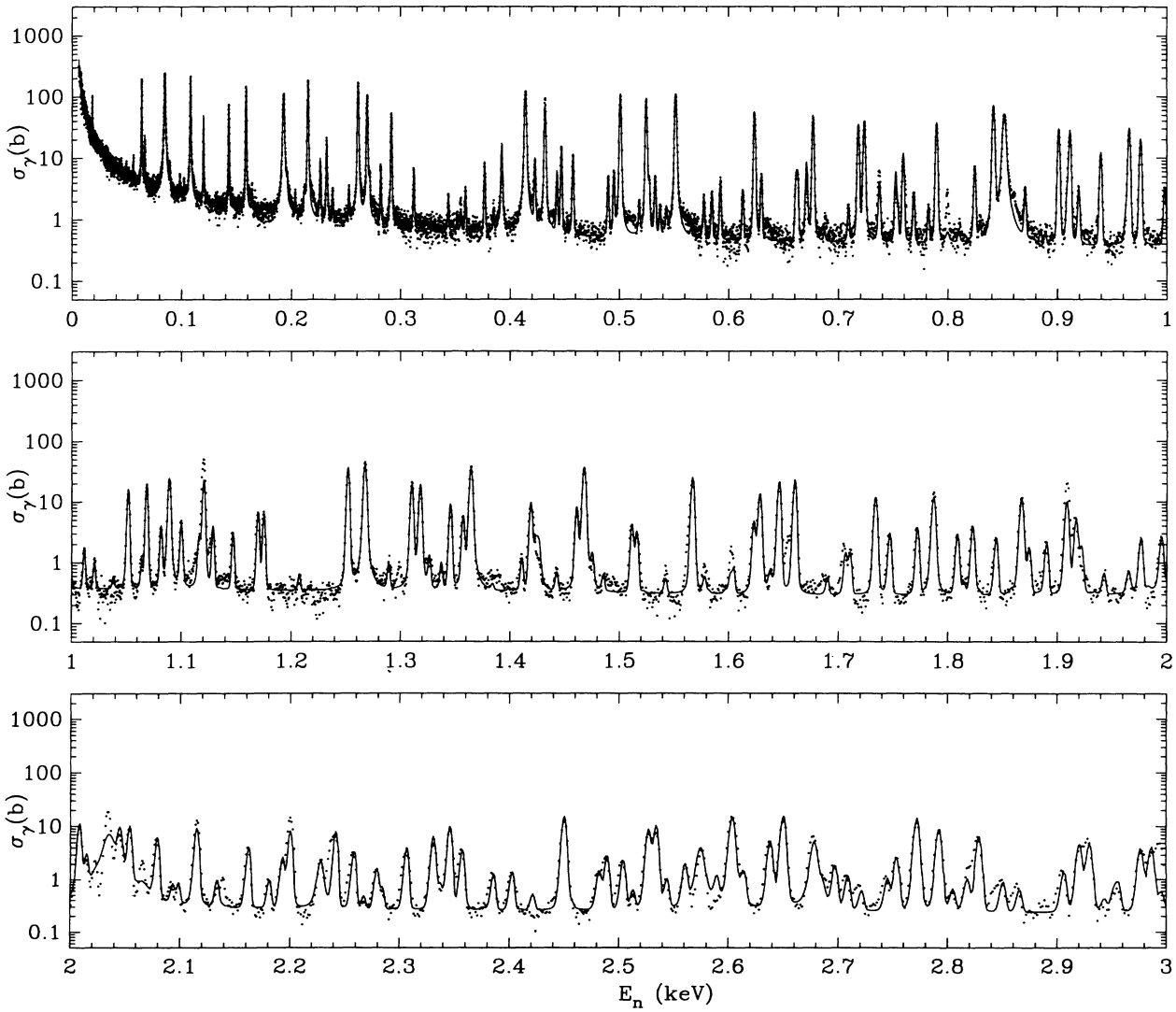

FIG. 3. ^{113}Cd capture data and fit from 0 to 3 keV. Data in between resonances must not be taken as capture cross sections: See explanation in the text.

TABLE IV. Neutron resonance parameters of ^{113}Cd up to 1 keV.

E_n (eV)	ℓ	$g\Gamma_n$ (meV)	$g\Gamma_n^\ell$ (meV)
0.178[a] ± 0.002	0	0.49 ± 0.03	1.15 ± 0.05
7.00[b] ± 0.01	1	0.00031 ± 0.00003	8.2 ± 0.8
18.365 ± 0.004	0	0.141 ± 0.001	0.0329 ± 0.0002
21.831 ± 0.007	1	0.0071 ± 0.0002	33.7 ± 0.9
43.38 ± 0.03	1	0.0047 ± 0.0004	8.0 ± 0.7
49.77 ± 0.01	1	0.0150 ± 0.0005	20.8 ± 0.7
56.23 ± 0.01	1	0.0403 ± 0.0006	46.5 ± 0.7
63.70 ± 0.01	0	2.60 ± 0.03	0.326 ± 0.004
81.52 ± 0.03	1	0.0054 ± 0.0004	3.6 ± 0.3
84.91 ± 0.02	0	22.4 ± 0.1	2.43 ± 0.01
98.52 ± 0.02	1	0.042 ± 0.001	20.9 ± 0.5
102.30 ± 0.02	1	0.037 ± 0.001	17.4 ± 0.5
106.56 ± 0.02	1	0.030 ± 0.002	13.3 ± 0.9
108.33 ± 0.02	0	8.52 ± 0.06	0.819 ± 0.006
143.07 ± 0.03	0	2.34 ± 0.03	0.196 ± 0.003
158.76 ± 0.03	0	6.47 ± 0.06	0.514 ± 0.005
166.60 ± 0.13	1	0.020 ± 0.002	4.5 ± 0.5
192.85 ± 0.04	0	45.8 ± 0.1	3.30 ± 0.01
196.15 ± 0.04	1	0.100 ± 0.005	17.6 ± 0.9
203.51 ± 0.04	1	0.067 ± 0.003	11.2 ± 0.5
211.88 ± 0.05	1	0.078 ± 0.003	12.3 ± 0.5
215.23 ± 0.05	0	20.2 ± 0.1	1.377 ± 0.007
232.41 ± 0.05	0	1.06 ± 0.01	0.069 ± 0.001
237.87 ± 0.05	1	0.125 ± 0.004	16.6 ± 0.5
252.68 ± 0.05	1	0.140 ± 0.004	17.0 ± 0.5
261.07 ± 0.06	0	26.3 ± 0.2	1.63 ± 0.01
269.35 ± 0.06	0	17.5 ± 0.1	1.066 ± 0.006
271.50 ± 0.06	1	0.26 ± 0.01	28.3 ± 0.8
281.83 ± 0.06	0	0.482 ± 0.006	0.0290 ± 0.0004
289.64 ± 0.09	1	0.060 ± 0.006	5.9 ± 0.6
291.61 ± 0.06	0	4.40 ± 0.07	0.258 ± 0.004
312.30 ± 0.07	1	0.491 ± 0.007	43.3 ± 0.6
343.79 ± 0.07	1	0.17 ± 0.01	13.0 ± 0.8
351.61 ± 0.19	1	0.036 ± 0.003	2.7 ± 0.2
359.32 ± 0.08	1	0.28 ± 0.01	20.0 ± 0.7
376.82 ± 0.08	1	0.83 ± 0.01	59.3 ± 0.7
385.01 ± 0.12	1	0.089 ± 0.006	5.7 ± 0.4
414.05 ± 0.09	0	94.5 ± 0.4	4.64 ± 0.02
422.73 ± 0.09	1	1.00 ± 0.02	56 ± 1
432.01 ± 0.09	0	18.3 ± 0.2	0.88 ± 0.01
447.11 ± 0.09	0	2.10 ± 0.02	0.099 ± 0.001
457.75 ± 0.10	0	1.62 ± 0.02	0.076 ± 0.001
489.89 ± 0.10	1	0.72 ± 0.02	32.3 ± 0.9
495.08 ± 0.10	0	0.91 ± 0.01	0.041 ± 0.001
501.0 ± 0.1	0	36.9 ± 0.3	1.65 ± 0.01
518.3 ± 0.1	1	0.21 ± 0.01	8.7 ± 0.4
524.8 ± 0.1	0	26.1 ± 0.3	1.14 ± 0.01
527.4 ± 0.1	1	0.72 ± 0.01	28.9 ± 0.4
533.0 ± 0.1	1	0.75 ± 0.02	29.7 ± 0.8
537.5 ± 0.2	1	0.18 ± 0.01	7.0 ± 0.4
543.3 ± 0.3	1	0.18 ± 0.01	6.9 ± 0.4
551.9 ± 0.1	0	79.3 ± 0.5	3.38 ± 0.02
577.6 ± 0.1	1	0.37 ± 0.02	13.0 ± 0.7
584.7 ± 0.1	1	0.47 ± 0.02	16.2 ± 0.7
592.5 ± 0.1	1	0.85 ± 0.02	28.7 ± 0.7
613.0 ± 0.1	1	0.58 ± 0.02	18.6 ± 0.6
623.7 ± 0.1	0	15.4 ± 0.2	0.617 ± 0.008
629.9 ± 0.1	0	1.20 ± 0.02	0.048 ± 0.001
661.3 ± 0.1	1	1.04 ± 0.02	29.8 ± 0.6
662.9 ± 0.1	0	1.46 ± 0.03	0.057 ± 0.001

TABLE IV. *(Continued).*

E_n (eV)	ℓ	$g\Gamma_n$ (meV)	$g\Gamma_n^\ell$ (meV)
677.1 ± 0.3	0	14.9 ± 0.2	0.573 ± 0.008
687.6 ± 0.2	1	0.06 ± 0.01	1.6 ± 0.3
709.3 ± 0.2	1	0.34 ± 0.02	8.8 ± 0.5
718.2 ± 0.2	0	11.6 ± 0.2	0.433 ± 0.008
723.6 ± 0.2	0	14.7 ± 0.2	0.547 ± 0.008
754.0 ± 0.2	1	0.34 ± 0.02	8.0 ± 0.5
759.3 ± 0.2	0	3.61 ± 0.04	0.131 ± 0.002
768.9 ± 0.2	1	0.78 ± 0.02	17.8 ± 0.5
782.2 ± 0.2	1	0.38 ± 0.02	8.5 ± 0.4
789.8 ± 0.2	0	14.4 ± 0.3	0.51 ± 0.01
824.6 ± 0.2	0	2.67 ± 0.05	0.093 ± 0.002
829.4 ± 0.5	1	0.12 ± 0.01	2.4 ± 0.2
841.7 ± 0.2	0	57.5 ± 0.6	1.98 ± 0.02
851.7 ± 0.2	0	401 ± 1	13.74 ± 0.03
870.6 ± 0.2	1	0.87 ± 0.03	16.5 ± 0.6
901.4 ± 0.2	0	14.6 ± 0.2	0.486 ± 0.007
911.7 ± 0.2	0	20.0 ± 0.3	0.66 ± 0.01
919.7 ± 0.2	1	1.01 ± 0.03	17.6 ± 0.5
939.7 ± 0.2	0	5.1 ± 0.3	0.17 ± 0.01
965.5 ± 0.2	0	13.4 ± 0.2	0.431 ± 0.006
976.0 ± 0.2	0	9.1 ± 0.4	0.29 ± 0.01
998.0 ± 0.2	1	1.59 ± 0.05	24.5 ± 0.8

[a]Parameters of this resonance taken from Ref. [7].
[b]Parameters of this resonance taken from Ref. [3].

that for resonances above 4 keV the reduced widths are calculated as if the resonances were $\ell = 0$.

IV. STATISTICAL TESTS OF THE DATA

The choice of which levels to assign as $\ell = 1$ as opposed to $\ell = 0$ is very difficult in an experiment such as this, where no direct evidence is obtained for the angular momentum of a particular resonance. In addition, as one moves to higher neutron energies the relative strength of the $\ell = 1$ resonances approaches that of the $\ell = 0$ resonances. Consequently, whereas at low energy one may be able to assign a resonance as $\ell = 1$ simply because it is far too weak to be $\ell = 0$ at higher energies, this distinction is blurred. We have attempted to assign levels to either $\ell = 0$ or 1 based on their widths. As an aid we have used the Bayes' theorem approach of Bollinger and Thomas [9].

The approach relies on the validity of the Porter-Thomas distribution for neutron widths and on the preliminary information on the strength functions S_ℓ and the level spacings D_ℓ. In order to calculate the preliminary strength functions we use the following relations for the reduced neutron widths:

$$g\Gamma_n^\ell = \frac{[1+(kR)^{2\ell}]g\Gamma_n}{(kR)^{2\ell}\sqrt{E(\mathrm{eV})}} = c^\ell(E)g\Gamma_n$$

where k is the neutron wave number and R is the nuclear radius. The c^ℓ parameters are

$$c^1(E) = \frac{5.7\times 10^5}{E(\mathrm{eV})\sqrt{E(\mathrm{eV})}}$$

and

$$c^0(E) = \frac{1}{\sqrt{E(\mathrm{eV})}}$$

for ^{113}Cd. For the level density we have used the $(2J+1)$ scaling law such that $D_1 = 4/9D_0$. The Bayes probability $P(E, g\Gamma_n, S_0, S_1, D_0)$ for a level with energy E and neutron width $g\Gamma_n$ to be p-wave is then given by

$$P = \frac{1}{1+\frac{4}{9}\sqrt{\frac{4}{3}\frac{c^0(E)}{c^1(E)}\frac{S^1}{S^0}}\exp\left[-\frac{g\Gamma_n}{2}\frac{c^0(E)}{D_0}\left(\frac{1}{S^0}-\frac{3}{4S^1}\frac{c^1(E)}{c^0(E)}\right)\right]}. \quad (1)$$

This probability is the relative probability normalized to the sum of s-wave and p-wave probabilities. With equal Porter-Thomas s-wave and p-wave probabilities, the Bayesian probability is $P = 0.69$ due to the *a priori* factor of 9/4 in favor of the p-wave assignement. Therefore, we have chosen to label resonances, which have a Bayesian probability of being $\ell = 1$ greater than 0.69, as $\ell = 1$. Of course, the assignment is not reliable for cases with the probability values near 0.69. In such cases we have used additional information on the observed distributions of neutron width and level spacings. Above 4 keV it became impossible to follow this procedure, and we have therefore not assigned any angular momentum values.

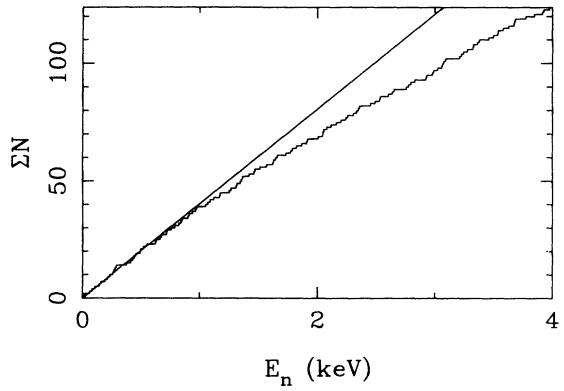

FIG. 4. Cumulative level count for resonances assigned as $\ell = 0$.

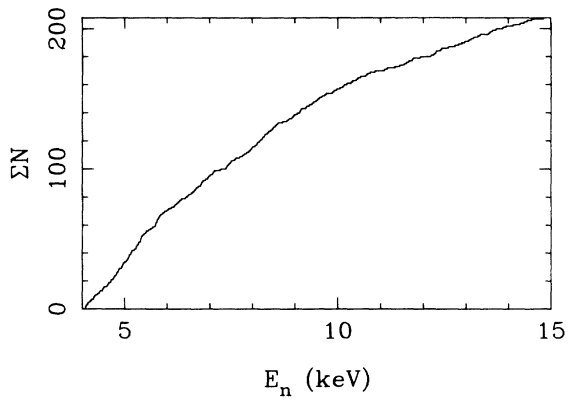

FIG. 6. Cumulative level count for resonances between 4 keV and 15 keV.

Figures 4 and 5 give plots of the cumulative number of levels for the s-wave and p-wave resonances, respectively. Levels between 4 keV and 15 keV are shown in Fig. 6 to illustrate the observed level density in that region. We have used the interval 0 to 1.5 keV to calculate the level density. The number of observed s-wave levels was corrected by the missing fraction obtained from the Porter-Thomas distribution. The p-wave level spacing was then calculated from the s-wave level spacing using the ratio of 4:9. The calculated level spacing of $\langle D_0 \rangle = 24.8 \pm 2.6$ eV for the s-wave resonances is in agreement with the the value of 22.1 ± 3.8 eV given by Liou *et al.* [2]. It is obvious from inspection that a greater number of levels is missed as the neutron energy increases. Similarly, the p-wave level spacing of $\langle D_1 \rangle = 11.0 \pm 1.2$ eV is in reasonable agreement with the earlier work [4] on the p-wave resonances.

The neutron strength functions S_ℓ are defined as

$$S_\ell = \frac{\langle g\Gamma_n^\ell \rangle}{(2\ell+1)\, D_\ell} = \frac{1}{(2\ell+1)\, \Delta E} \sum_{i=1}^{N} g_i \Gamma_{ni}^\ell, \qquad (2)$$

where the summation is over the N resonances with the proper ℓ value in the interval ΔE. Such strength functions were found for both the $\ell = 0$ and $\ell = 1$ resonances.

The s-wave strength function to $E_{\max} = 15$ keV is given in Fig. 7 and the p-wave strength function to $E_{\max} = 1$ keV is given in Fig. 8. The strength functions are computed from the slopes of the fitted lines. Note that the levels between 4 keV and 15 keV are included in the computation of the s-wave strength function, since the levels that contribute significantly in this case will be predominantly s-wave. The s-wave strength function is found to be $10^4 S_0 = 0.32 \pm 0.02$, while the p-wave strength function is $10^4 S_1 = 3.0 \pm 0.5$. The uncertainties are calculated as $\pm 1.4/\sqrt{n}$. Both are in agreement with earlier work [2,4].

The neutron reduced widths are expected to obey the Porter-Thomas [16] distribution

$$P(y) = \frac{e^{\frac{-y}{2}}}{\sqrt{2\pi y}}, \qquad (3)$$

where $y = \gamma_i^2/\gamma_{\rm av}^2$, γ_i^2 is the neutron reduced width for the ith resonance in either the s-wave or p-wave sequence, and $\gamma_{\rm av}^2$ is the average neutron reduced width in the same sequence. In the absence of information on resonance spins, we believe that S_ℓ does not depend on spin and use $\gamma^2 = g\Gamma_n^\ell$ and $\gamma_{\rm av}^2 = \langle g\Gamma_n^\ell \rangle$. In order to avoid the confusion associated with the choice of bin widths in a

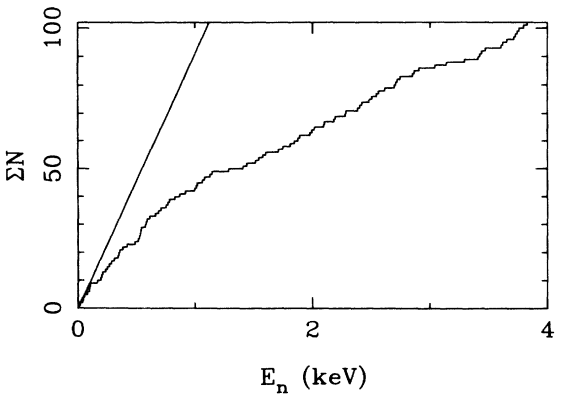

FIG. 5. Cumulative level count for resonances assigned as $\ell = 1$.

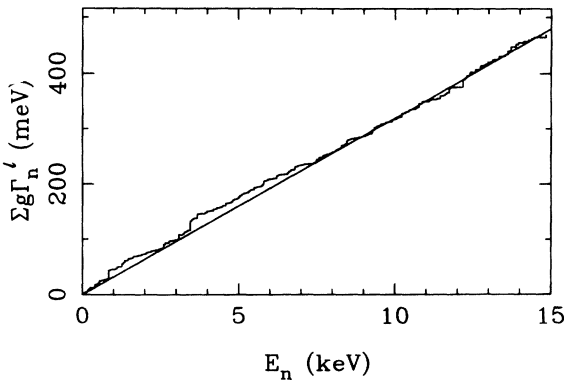

FIG. 7. $\sum g\Gamma_n^0$ vs neutron energy for the ^{113}Cd s-wave levels.

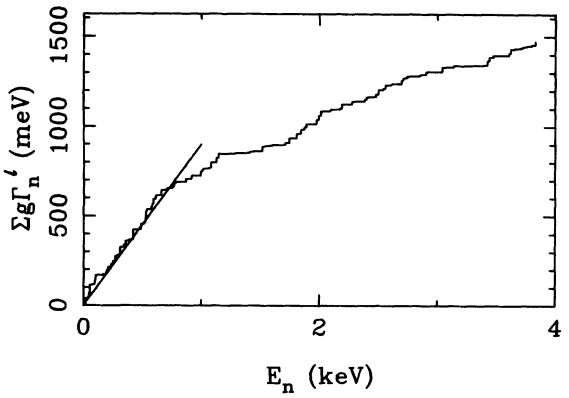

FIG. 8. $\sum g\Gamma_n^1$ vs neutron energy for the ^{113}Cd p-wave levels.

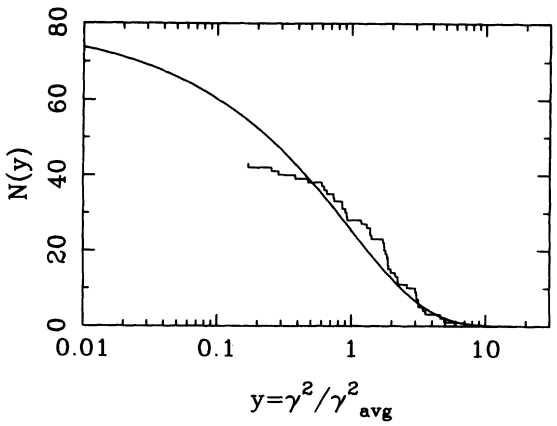

FIG. 10. Cumulative reduced width distribution compared with the integral of the Porter-Thomas distribution for the p-wave sequence (0–1 keV).

histogram distribution, we choose to consider the cumulative reduced width distribution. The experimental distributions for the s-wave resonances up to 4 keV and the p-wave resonances up to 1 keV are shown in Figs. 9 and 10 along with the integral of the Porter-Thomas distribution. Examination of the figures reveals that a number of levels are missed in both sequences and that in both cases there is a clear minimum reduced width that is observable. A bootstrap analysis [17] of the missing fraction of s-wave levels indicates that approximately 13% of the s-wave levels are missed up to 1.5 keV. A simple comparison between the number of p-wave levels observed up to 1.5 keV and the number expected by scaling the number of s-wave levels by $\frac{2}{4}$ would indicate that greater than 50% of the p-wave levels are missed.

Nearest neighbor spacing distributions for levels of the same symmetry are expected to obey the Wigner [18] distribution

$$P(x) = \frac{\pi}{2} x e^{\frac{-\pi x^2}{4}}. \tag{4}$$

The spacing parameter $x = D_i/\langle D\rangle$, where $D_i = (E_{i+1} - E_i)$ and $\langle D\rangle$ is the average level spacing. For sequences with more than one J value, the appropriate mixed distribution must be constructed. The s-wave sequence consists of $J = 0$ and 1 and the p-wave sequence consists of $J = 0$, 1, and 2. The appropriate mixed distribution is composed of two (three) pure Gaussian orthogonal ensemble (GOE) sequences for $J = 0$ and 1 (and 2) with relative level densities of 1 and 3 (and 5) for the s-wave (p-wave) sequence. In Figs. 11 and 12 the cumulative spacing distributions are shown for the s-waves up to 4 keV and for the p-waves up to 1 keV. The predictions for the Poisson, Wigner, and mixed distributions are also shown for comparison. The s-wave sequence lies between the Poisson distribution and the mixed distribution, indicating that the sequence is not perfect. For the p-wave sequence the agreement is clearly with the Poisson distribution.

Nuclear level sequences of very high quality have fluctuation properties, which agree with the predictions of the Gaussian orthogonal ensemble (GOE) of random matrix theory [19–21]. The s-wave sequence should be expected to give reasonable agreement with the GOE if the

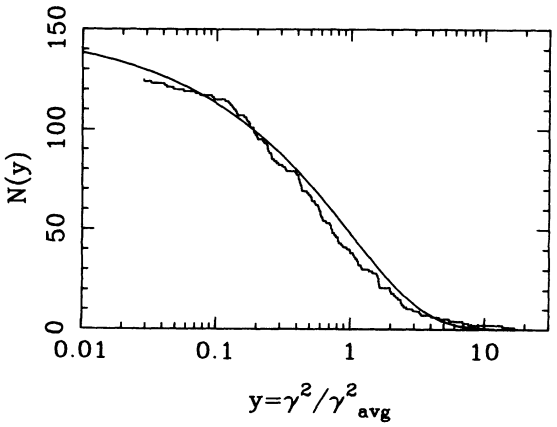

FIG. 9. Cumulative reduced width distribution compared with the integral of the Porter-Thomas distribution for the s-wave sequence (0–4 keV).

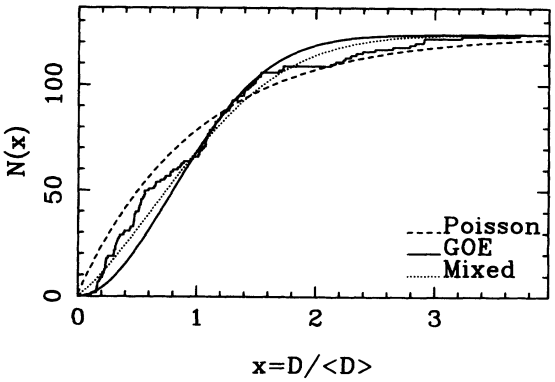

FIG. 11. Cumulative nearest neighbor spacing distributions compared with the Wigner, Poisson, and mixed GOE sequences for the s-wave resonances up to 4 keV. Note that there are two sequences combined ($J = 0, 1$) with relative densities of 1 and 3.

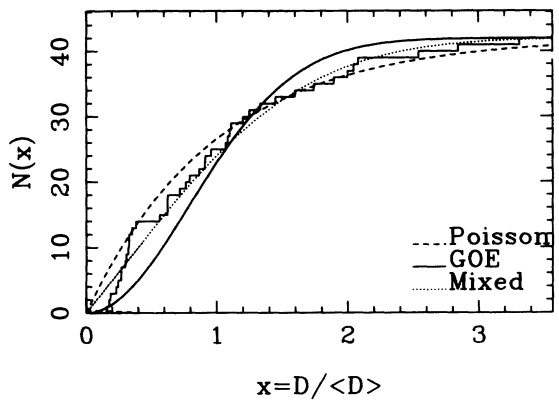

FIG. 12. Cumulative nearest neighbor spacing distributions compared with the Wigner, Poisson, and mixed GOE sequences for the p-wave resonances up to 1 keV. Note that there are three sequences combined (J=0,1,2) with relative densities of 1, 3, and 5.

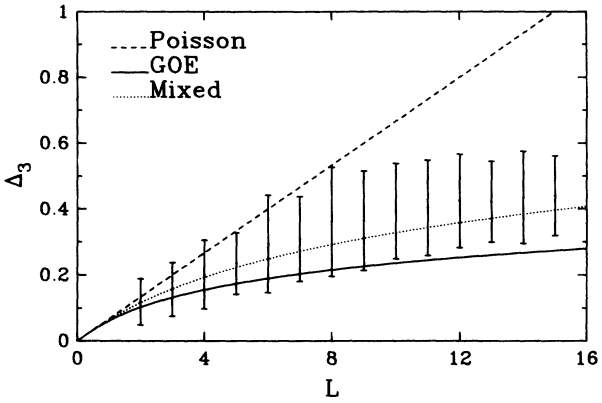

FIG. 13. The Δ_3 statistic for the s-wave resonances up to 4 keV. The solid curve is for one pure GOE sequence, the dashed curve for a Poisson sequence, and the dotted curve for two GOE sequences mixed with relative densities of 1 and 3.

sequence is sufficiently pure. Almost certainly too many levels are missed in the p-wave sequence for it to be expected to agree with the GOE. The most used simple test of the fluctuation properties is the Dyson-Metha Δ_3 statistic [22]. The Δ_3 statistic for a sequence of levels with the same J, π, and ℓ (in general all quantum numbers should be the same; in practice J, π, and ℓ suffice) between energies $E_{\min}$ and $E_{\max}$ is

$$\Delta_3(L) = \min_{A,B} \frac{1}{E_{\max} - E_{\min}} \times \int_{E_{\min}}^{E_{\max}} [N(E) - AE - B]^2 dE, \quad (5)$$

where $N(E)$ is the number of levels in the interval $[E_{\min}, E_{\max}]$ with energies less than or equal to E, and L is an integer. For a given L the energy region is subdivided into intervals of length $L\langle D\rangle$, which overlap by $L\langle D\rangle/2$. A value for Δ_3 is calculated for each interval, and the value of Δ_3 for a given L is then the average of Δ_3 for all intervals of size $L\langle D\rangle$. For the GOE the expected value is approximately

$$\Delta_{3\mathrm{GOE}} \cong \frac{1}{\pi^2}[\ln L - 0.068], \quad (6)$$

while for Poisson statistics the expected value is $L/15$. As with the previous test, one must consider the data for Δ_3 with a mixed sequence of two (three) sequences combined for the s-wave (p-wave) resonances. Such mixed sequences were constructed using the same relative level densities mentioned above. The data for the s-wave levels up to 4 keV are shown in Fig. 13, along with the computed Δ_3 for Poisson, GOE, and mixed sequences. There is clear agreement between the data and the mixed sequence computation. For the case of the p-wave resonances up to 1 keV (Fig. 14) the errors are sufficiently large that they could be said to agree with either the mixed or the Poisson distributions, though the trend is toward the Poisson distribution. Because of the large number of missed levels in the p-wave sequence, one would expect the Δ_3 data to agree with a Poisson distribution.

An additional statistic one may consider is the linear correlation coefficient between adjacent spacings. The linear correlation coefficient is defined as

$$\rho(x,y) = \frac{\sum_i (x_i - \langle x\rangle)(y_i - \langle y\rangle)}{\left[\sum_i (x_i - \langle x\rangle)^2 \sum_i (y_i - \langle y\rangle)^2\right]^{1/2}}. \quad (7)$$

The value of the correlation coefficient ranges between -1 and $+1$. For GOE spacing the expected value is -0.27 [23], while for Poisson no correlation is expected ($\rho = 0$). The correlation coefficient for both the s-wave and p-wave sequences was investigated as a function of energy. Each sequence was considered in larger and larger regions, starting with 0–500 eV and going until the sequence ended. The coefficients are displayed in Table V.

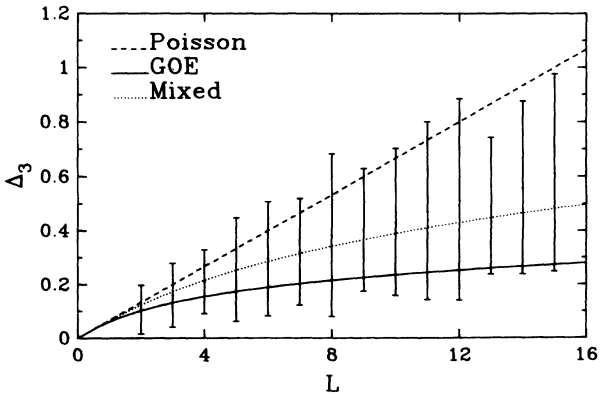

FIG. 14. The Δ_3 statistic for the p-wave resonances up to 1 keV. The solid curve is for one pure GOE sequence, the dashed curve for a Poisson sequence, and the dotted curve for three GOE sequences mixed with relative densities of 1, 3, and 5.

TABLE V. The linear correlation coefficient ρ for s-wave and p-wave sequences as a function of energy region.

Energy region (keV)	$\rho_{s\text{-}wave}$	$\rho_{p\text{-}wave}$
$0 \rightarrow 0.5$	$-0.16^{+0.27}_{-0.29}$	$+0.21^{+0.24}_{-0.27}$
$0 \rightarrow 1.0$	$-0.27^{+0.14}_{-0.17}$	$+0.34^{+0.14}_{-0.14}$
$0 \rightarrow 2.0$	$-0.26^{+0.11}_{-0.10}$	$+0.25^{+0.16}_{-0.20}$
$0 \rightarrow 3.0$	$-0.25^{+0.07}_{-0.08}$	$+0.00^{+0.14}_{-0.15}$
$0 \rightarrow 4.0$	$-0.19^{+0.08}_{-0.07}$	$+0.16^{+0.12}_{-0.14}$

Note that the s-wave sequence starts out being consistent with the GOE but starts to diverge slightly after a few keV. This can be ascribed to missing a larger and larger fraction of the levels as the energy increases. The correlation coefficient for the p-waves is generally consistent with zero. However, the large indicated errors do not allow one to make a definite conclusion.

V. SUMMARY

We have investigated the neutron resonances in ^{113}Cd up to $E_n = 15$ keV. A total of 377 levels have been added to those known in ^{113}Cd. Resonance parameters have been extracted for all 437 known levels. Various statistical tests of the data indicate the high quality of the data at low energies with virtually no missed levels, while at higher energies the quality of the data deteriorates. The measured strength functions and level spacings are consistent with earlier measurements and have significantly greater accuracy.

The spectroscopic information obtained on the ^{113}Cd neutron resonance parameters is indispensable in obtaining the weak matrix elements from the corresponding parity violation effects recently found in some p-wave resonances of this nucleus. The results obtained encourage the experimenters to perform the parity violation measurements in a broader energy region. Moreover, the agreement of the data with the statistical tests gives confidence in applying the statistical model to the parity violation phenomenon in highly excited states of ^{113}Cd.

ACKNOWLEDGMENTS

This work was supported by the U.S. Department of Energy under Contract Nos. W-7405-ENG-36 (Los Alamos National Laboratory) and DE-AC05-84OR21400 (Oak Ridge National Laboratory).

[1] Yu.G. Abov, P.A. Krupchitsky, and Y.A. Oratovsky, Phys. Lett. **12**, 25 (1964).
[2] H.I. Liou, G. Hacken, F. Rahn, J. Rainwater, M. Slagowitz, and W. Makofske, Phys. Rev. C **10**, 709 (1974).
[3] V.P. Alfimenkov, S.B. Borzakov, Yu.D. Mareev, L.B. Pikelner, V.R. Skoy, A.S. Khrykin, and E.I. Sharapov, Yad. Fiz. **52**, 927 (1990) [Sov. J. Nucl. Phys. **52**, 589 (1990)]. See also, Joint Institute for Nuclear Research Report P-3-87-117, Dubna, 1987.
[4] C.M. Frankle, C.D. Bowman, J.D. Bowman, S.J. Seestrom, E.I. Sharapov, Yu.P. Popov, and N.R. Roberson, Phys. Rev. C **45**, 2143 (1992).
[5] S.J. Seestrom *et al.*, ISINN-2 Abstracts (2nd International Seminar on Interaction of Neutrons with Nuclei), Dubna (1994), p. 17.
[6] J.W.T. Dabbs, *Nuclear Cross Sections for Technology*, NBS Special Publication 594, (U.S. GPO, Washington, DC, 1980), p. 929.
[7] S.F. Mughabghab, M. Divadeenam, and N.E. Holden, *Neutron Cross Sections* (Academic, New York, 1981), Vol. 1A.
[8] N.M. Larson, Oak Ridge National Laboratory Report TM-9179/R2, 1989.
[9] L.M. Bollinger and G.E. Thomas, Phys. Rev. **171**, 1293 (1968).
[10] R.L. Macklin, Nucl. Instum. Methods **91**, 79 (1971).
[11] R.L. Macklin, N.W. Hill, J.A.Harvey, and G.L. Tweed, Phys. Rev. C **48**, 1120 (1993).
[12] H. Beer and R.L. Macklin, Phys. Rev. C **26**, 1404 (1982).
[13] R.L. Macklin, J. Halperin, and R.R. Winters, Nucl. Instrum. Methods **164**, 213 (1979).
[14] C.W. Reich and M.S. Moore, Phys. Rev. **111**, 929 (1958).
[15] "See AIP document no. PAPS PRVCA-50-2774-12 for 12 pages of tables. Order by PAPS number and journal reference from American Institute of Physics, Physics Auxiliary Publication Service, Carolyn Gehlbach, 500 Sunnyside Boulevard, Woodbury, New York, 11797. Fax: 516-576-2223, e-mail: janis@aip.org. The price is $1.50 for each microfiche (98 pages) or $5.00 for photocopies of up to 30 pages, and $0.15 for each additional page over 30 pages. Airmail additional. Make checks payable to the American Institute of Physics."
[16] C.E. Porter and G.E. Thomas, Phys. Rev. **104**, 483 (1956).
[17] B. Efron, SIAM (Soc. Ind. Appl. Math.) Rev. **21**, 460 (1979).
[18] E.P. Wigner, in Proceedings of the Canadian Mathematical Congress, 1957 (unpublished); see also J.E. Lynn, *The Theory of Neutron Resonance Reactions* (Clarendon, Oxford, 1968).
[19] T.A. Brody, J. Flores, J.B. French, P.A. Mello, A. Pandey, and S.S.M. Wong, Rev. Mod. Phys. **53**, 385 (1981).
[20] R. U. Haq, A. Pandey, and O. Bohigas, Phys. Rev. Lett. **48**, 1086 (1985).
[21] O. Bohigas, R.U. Haq, and A. Pandey, Phys. Rev. Lett. **54**, 1645 (1985).
[22] F.J. Dyson and M.L. Metha, J. Math. Phys. **4**, 701 (1963).
[23] M.L. Mehta, in *Statistical Properties of Nuclei* (Plenum, New York, 1972), p. 179.